The influence of Kondo physics on the properties of a spin glass

2008 J. Phys.: Condens. Matter 20 095202

(http://iopscience.iop.org/0953-8984/20/9/095202)

J. Phys.: Condens. Matter **20** (2008) 095202 (6pp) doi:10.1088/0953-8984/20/9/095202

The influence of Kondo physics on the properties of a spin glass

Farhad Fazileh and Eugene H Kim

Department of Physics, University of Windsor, Windsor, ON, N9B 3P4, Canada

Received 26 October 2007, in final form 16 January 2008
Published 4 February 2008
Online at stacks.iop.org/JPhysCM/20/095202

Abstract

The influence of Kondo physics on the properties of a spin glass is considered. Numerical results obtained on a $20 \times 20 \times 20$ lattice are presented for the magnetization, the distribution of fields, and the impurity spin susceptibility in the spin glass phase. We discuss how these quantities depend on the system's history; we show how they are influenced by Kondo physics.

(Some figures in this article are in colour only in the electronic version)

1. Introduction

The problem of magnetic impurities in metals has been of considerable interest for some time [1]. The interaction between the conduction electrons and the magnetic impurities is described by the Kondo Hamiltonian [2]

$$H_{\text{Kondo}} = J \sum_i \tau_i \cdot \mathbf{S}(\mathbf{r}_i). \tag{1}$$

In equation (1), τ_i is the spin operator of the ith impurity (located at $\mathbf{r}_i$); $\mathbf{S}(\mathbf{r}_i)$ is the conduction electrons' spin operator at $\mathbf{r}_i$; J is the exchange interaction between the conduction electrons and the magnetic impurities. For the rest of this work, we will focus on the case of spin-1/2 impurities; we will take the exchange interaction to be antiferromagnetic $J > 0$.

Magnetic impurities cause spin-flip scattering of the conduction electrons; they give rise to the Kondo effect with its dynamically generated scale, the Kondo temperature T_{K} [1]. The physics behind this dynamically generated scale is a correlated many-body state, where the impurity spin is locked in a singlet with a cloud of electrons—the Kondo screening cloud. Besides the Kondo effect, the conduction electrons mediate an effective interaction between impurities—the Ruderman–Kittel–Kasuya–Yosida (RKKY) interaction [3]—given by

$$H_{\text{RKKY}} = -\tfrac{1}{2} \sum_{i \neq j} K_{i,j}\, \tau_i \cdot \tau_j. \tag{2}$$

As the impurities are in random positions, it is a random interimpurity interaction. This random interaction drives the system into a spin glass phase, having a complex free-energy landscape with many metastable states.

Recently, the resistivity $\rho(T)$ of gold wires doped with very dilute amounts of iron was measured; signs of both the Kondo effect and spin glass physics were observed in $\rho(T)$ [4]. In these systems, the concentration of iron was more dilute than in alloys where spin glass physics was observed previously; in describing these systems, a proper treatment of both the Kondo effect as well as spin glass physics is necessary. Motivated by these experiments, we would like to understand the interplay between the Kondo effect and spin glass physics i.e. the interplay between equations (1) and (2). We would particularly like to understand the properties of partially screened impurities and the effects of coherence between partially screened impurities.

The rest of this paper is organized as follows. In section 2, we describe the model considered in this work and the approach employed to treat the model. Section 3 presents results obtained numerically on a $20 \times 20 \times 20$ lattice, showing how the properties of the spin glass phase are influenced by Kondo physics. In particular, we first investigate hysteresis in the field-dependent magnetization in the glass phase. We then present results for the distribution of internal fields and discuss its history dependence. Finally, we present results for the impurity spin susceptibility. Previous work studying the interplay of random interimpurity interactions and the Kondo effect employed the replica formalism [5]. These works focused on the 'replica-symmetric' phase(s); the properties of the glass phase itself were not discussed. Works which did consider the properties within the glass phase did not take into account the Kondo effect [6–8]. Section 4 presents some concluding remarks.

2. The model and approach

To make progress, we consider an anisotropic limit of the exchange coupling in equation (1): $J^{xy} \neq J^z$. It is known

that the Kondo Hamiltonian with $J^{xy} \neq J^z$ has the same low-energy physics as the isotropic limit. Furthermore, rather than consider a collection of randomly placed impurities, we follow other works and put the impurity spins on a cubic lattice; we take the $\{K_{i,j}\}$ to be Gaussian distributed random variables between nearest neighbor sites

$$\mathcal{P}(K_{i,j}) = \sqrt{\frac{1}{2\pi K^2}} \exp\left[-K_{i,j}^2/2K^2\right]. \tag{3}$$

Finally, to simplify the analysis, we take the interimpurity interaction in equation (2) to be an Ising interaction. Physically, such an interaction could arise due to crystal field effects. More generally, interactions which break the spin $SU(2)$ symmetry are known to give rise to Ising-like behavior, as these interactions make it difficult for the impurity spins to rotate [6]. Therefore, the Hamiltonian we consider is $H = H_0 + H_{\rm imp}$, where H_0 is the free Hamiltonian of the conduction electrons and

$$H_{\rm imp} = J^{xy} \sum_i \left[\tau_i^+ S^-(\mathbf{r}_i) + \tau_i^- S^+(\mathbf{r}_i)\right] + J^z \sum_i \tau_i^z S^z(\mathbf{r}_i) - H_z \sum_i \tau_i^z - \tfrac{1}{2} \sum_{i\neq j} K_{i,j}\, \tau_i^z \tau_j^z. \tag{4}$$

Note that in equation (4), we have included an external magnetic field H_z acting on the impurity spins.

To analyze the physics, we treat the RKKY interaction in mean-field theory. This approach, which is motivated by the seminal work of [9], has been successfully used to study conventional spin glasses (where the Kondo effect is ignored) [7, 8]; it has recently been used to study history-dependent phenomena in the transverse field Ising glass [10]. In this approximation, $H_{\rm imp} \simeq \sum_{i=1}^N H_{\rm imp}^i$, where

$$H_{\rm imp}^i = J^{xy}\left[\tau_i^+ S^-(\mathbf{r}_i) + \tau_i^- S^+(\mathbf{r}_i)\right] + J^z \tau_i^z S^z(\mathbf{r}_i) + h_i\, \tau_i^z, \tag{5}$$

where $h_i = H_z + h_i^{\rm int}$ with

$$h_i^{\rm int} = \sum_j K_{i,j} \langle \tau_j^z \rangle \tag{6}$$

being an effective, random field acting on impurity-i due to the rest of the impurities. The $\{\langle \tau_j^z \rangle\}$ are to be determined self-consistently. As the fields $\{h_i\}$ are random, physical quantities must be averaged over the distribution of fields

$$\mathcal{P}(h_i) = \left\langle \delta\left(h_i - \sum_j K_{i,j}\, \langle \tau_j^z \rangle\right)\right\rangle_{K_{i,j}}, \tag{7}$$

where $\langle\ \rangle_{K_{i,j}}$ denotes averaging over the distribution of couplings $\{K_{i,j}\}$. Within this approach, information about the various phases which arise is contained in $\mathcal{P}(h_i)$.

A few words are in order about the mean-field approach utilized in this work. This approach is valid to describe the finite temperature properties within the glass phase. It is not expected to describe the properties at $T = 0$ or the critical behavior at a phase transition, as fluctuations are ignored. Furthermore, this approach is implicitly nonergodic and probes the system on intermediate timescales. This is because a particular minimum on the free-energy manifold (in which the spin glass was originally prepared) is followed with field and/or temperature. (See below.) As will be seen explicitly below, changes in field and temperature distort the free-energy manifold—minima of the free-energy become displaced or even disappear. Hence, on short timescales, the system may not have time to re-equilibrate after the field or temperature has been changed. On long timescales, however, thermal activation or/and tunneling will allow the system to find its way out of the minimum in which the system has been prepared.

To proceed further, we expand the conduction electron operator in spherical waves centered about each impurity. Furthermore, we approximate by ignoring the overlap between conduction electron wave functions centered about different impurities. This approximation is justified, provided the concentration of impurities is sufficiently dilute and the distances between impurities are large—the effects ignored are subleading [11]. In this approximation, each impurity is coupled to its own bath of conduction electrons. As we are taking the interaction between the conduction electrons and the impurity to occur at a point (see equation (5)), only a single harmonic—namely, the s-wave channel—couples to the impurity [12]. Focusing on this s-wave channel, we can write an effective one-dimensional model for the conduction electron bath centered about each impurity. Our Hamiltonian becomes $H = \sum_{i=1}^N H_i$ where $H_i = H_0^i + H_{\rm imp}^i$ with

$$H_0^i = -{\rm i} v_{\rm F} \int {\rm d}x\, \psi_{R,i,s}^\dagger \partial_x \psi_{R,i,s} + \cdots; \tag{8a}$$

$$H_{\rm imp}^i = 2\pi v_{\rm F} \lambda^{xy} \left[\tau_i^+ J_{R,i}^-(0) + \tau_i^- J_{R,i}^+(0)\right] + 2\pi v_{\rm F} \lambda^z \tau_i^z J_{R,i}^z(0) + h_i \tau_i^z. \tag{8b}$$

In equation (8*a*), $\psi_{R,i,s}$ destroys a (right-moving) electron with spin-s in the bath centered about the ith impurity; $v_{\rm F}$ is the Fermi velocity; the ellipses represent higher harmonics, which do not couple to the magnetic impurities. In equation (8*b*),

$$J_{R,i}^\alpha(0) = (1/2)\psi_{R,i,s}^\dagger(0) \sigma_{s,s'}^\alpha \psi_{R,i,s'}(0),$$

with $\{\sigma_{s,s'}^\alpha\}$ ($\alpha = x, y, z$) being the Pauli matrices; $\lambda^{xy} = J^{xy}\rho_0$ and $\lambda^z = J^z \rho_0$ are dimensionless couplings (ρ_0 is the conduction electrons' density-of-states).

In what follows, it will prove useful to utilize the boson representation of one-dimensional fermions [13]. To do so, the electron operator is written as $\psi_{R,i,s} \sim {\rm e}^{{\rm i}\sqrt{4\pi}\phi_{R,i,s}}$. It will also prove useful to form *charge* and *spin* fields $\phi_{R,i,\rho/\sigma} = (\phi_{R,i,\uparrow} \pm \phi_{R,i,\downarrow})/\sqrt{2}$. In terms of these variables,

$$H_i = v_{\rm F} \int {\rm d}x\, (\partial_x \phi_{R,i,\sigma})^2 + (\partial_x \phi_{R,i,\rho})^2 + \frac{v_{\rm F}\lambda^{xy}}{\alpha}\left[\tau_i^+ {\rm e}^{-{\rm i}\sqrt{8\pi}\phi_{R,i,\sigma}(0)} + \tau_i^- {\rm e}^{{\rm i}\sqrt{8\pi}\phi_{R,i,\sigma}(0)}\right] + v_{\rm F}\lambda^z \sqrt{2\pi}\, \tau_i^z\, \partial_x \phi_{R,i,\sigma}(0) + h_i\, \tau_i^z. \tag{9}$$

(α is a short-distance cut-off.) Notice that only the spin fields couple to the magnetic impurities; the charge fields decouple.

To treat the Kondo effect nonperturbatively, we perform a unitary transformation

$$U = \exp\left({\rm i}\beta \tau^z \phi_{R,i,\sigma}(0)\right)$$

with $\beta = \sqrt{\pi}(\sqrt{2}-1)$, which ties (part of) the conduction electrons' spin to the impurity [13]. Then, we introduce new fermion fields, $d_i \sim \tau_i^-$, and $\tilde{\psi}_{R,i} \sim e^{i\sqrt{4\pi}\phi_{R,i,\sigma}}$. Upon performing these transformations, H_i becomes

$$\begin{aligned} H_i = {} & v_F \int dx (\partial_x \phi_{R,i,\rho})^2 - i v_F \int dx \tilde{\psi}^\dagger_{R,i} \partial_x \tilde{\psi}_{R,i} \\ & + v_F \lambda^{xy} \sqrt{\frac{2\pi}{\alpha}} \left(d_i^\dagger \tilde{\psi}_{R,i}(0) + \tilde{\psi}^\dagger_{R,i}(0) d_i \right) \\ & + h_i \left(d_i^\dagger d_i - \frac{1}{2} \right) + v_F \sqrt{2\pi} \left[\lambda^z - \left(1 - \frac{1}{\sqrt{2}} \right) \right] \\ & \times \left(d_i^\dagger d_i - \tfrac{1}{2} \right) \tilde{\psi}^\dagger_{R,i}(0) \tilde{\psi}_{R,i}(0). \end{aligned} \tag{10}$$

For the remainder of this work, we will focus on the Toulouse point, $\lambda^z = 1 - 1/\sqrt{2}$. The Toulouse point is known to have the same low-energy fixed point as the $SU(2)$ symmetric Kondo model. However, the analysis simplifies at this point in parameter space—the marginally relevant operator near the ultraviolet fixed point (responsible for the Kondo logarithms) is fine-tuned away; similarly, the leading irrelevant operator near the infrared fixed point is also fine-tuned away [13].

3. Properties of the spin glass phase

From equation (10), we can readily understand how the properties of a spin glass are affected by Kondo physics. To properly describe the glass phases, $\langle \tau_i^z \rangle$ for the ith spin must be computed self-consistently, taking into account correlations with all the other $\{\langle \tau_j^z \rangle\} \forall j$. To this end, we perform a 'spatially-unrestricted mean-field' calculation to determine the $\{\langle \tau_i^z \rangle\}$ and, hence, the h_i in equation (6). Computing $\langle \tau_i^z \rangle$ using equation (10), we obtain

$$\langle \tau_i^z \rangle = \frac{1}{\pi} \mathrm{Im} \left[\psi \left(\frac{1}{2} + \frac{T_k}{4\pi T} + i \frac{h_i}{2\pi T} \right) \right],$$

where $\psi(z)$ is the digamma function [14], and $T_K = 2\pi v_F (\lambda^{xy})^2/\alpha$ is the Kondo temperature at the Toulouse point. Hence, the $\{h_i\}$ are determined by

$$h_i = H_z + \sum_{j \neq i} K_{i,j} \frac{1}{\pi} \mathrm{Im} \left[\psi \left(\frac{1}{2} + \frac{T_K}{4\pi T} + i \frac{h_j}{2\pi T} \right) \right]. \tag{11}$$

Equation (11) (which follows from equation (10)) is the central result of this work; the results presented in this section follow from numerical solutions of equation (11).

In equation (11), we are not considering the contribution from the reaction term. Similar to other works, we have found the reaction term to give severe problems with convergence [15]. It is well known that the mean-field equations without the reaction term overestimates the glass freezing temperature T_g [6, 9]; properties near the glass transition are not expected to be described correctly. Reference [16] considered a spin glass model where the reaction term vanishes; it was found that the properties near T_g were different from models where the reaction term must be considered. However, the model in [16] was found to have properties in the low temperature phase similar to models with a reaction term, namely a complex free-energy landscape with many metastable states. It has been found in studies of conventional spin glasses [7, 8] and also in the transverse field Ising glass [10] that the properties within the various phases and, particularly, the history-dependent phenomena are described reasonably well when the reaction term is not considered. Hence, equation (11) is expected to capture the essential physics of the glass phase in the model considered in this work.

To clearly discuss the influence of Kondo physics on the system, we formally consider the $T \to 0$ limit. By doing so, we are able to focus on the interplay between Kondo screening and interimpurity coherence i.e. the interplay between T_K and K. The results presented below were generated by considering impurity spins on a $20 \times 20 \times 20$ lattice, with equation (11) solved self-consistently at each site for various (random) configurations of the $\{K_{i,j}\}$ and different values of the external field H_z.

3.1. Hysteresis loops

We begin by considering the system's field-dependent magnetization M_z and, in particular, the hysteretic behavior exhibited by M_z in the spin glass phase. (M_z has been plotted as a fraction of M_0, the magnetization one would obtain if all the impurity spins are aligned.) This hysteretic behavior arises directly from the complexity of the free-energy manifold. Indeed, as the external field is varied, a given minimum of the free-energy becomes unstable and the system goes into a nearby minimum. As the free-energy manifold is very complex with many local minima, the system can find a new minimum with magnetization similar to the original minimum. The free-energy manifold becomes 'smoothed' (i.e. less complex), and the hysteretic behavior is lost as the moments become screened via the Kondo effect.

The hysteresis loops presented below were generated by preparing the system with different initial values of the external field and by sweeping the external field in different ways. In general, however, the calculation proceeded by preparing the impurity spins in a random configuration and with a particular value of the external field. Equation (11) was then used to obtain a self-consistent solution for the $\{h_i\}$. The external field was then gradually increased or decreased; the previously obtained (self-consistent) spin configuration was used as the starting seed in the calculations for the new value of the external field. This procedure to determine the $\{h_i\}$ was continued as the external field was swept until a complete hysteresis loop was generated.

Figure 1 shows hysteresis loops for various values of T_K, where the field was swept symmetrically. More specifically, the system was prepared in a random configuration in zero external field; the field was increased to a finite positive value $H_z/K = 15$. The external field was then decreased to $H_z/K = -15$, and finally increased back to $H_z/K = 15$, thus generating a complete hysteresis loop. We see that the hysteresis loops in figure 1 are broader for smaller values of T_K; they become narrower as T_K increases. Eventually, the hysteretic behavior disappears for T_K sufficiently large,

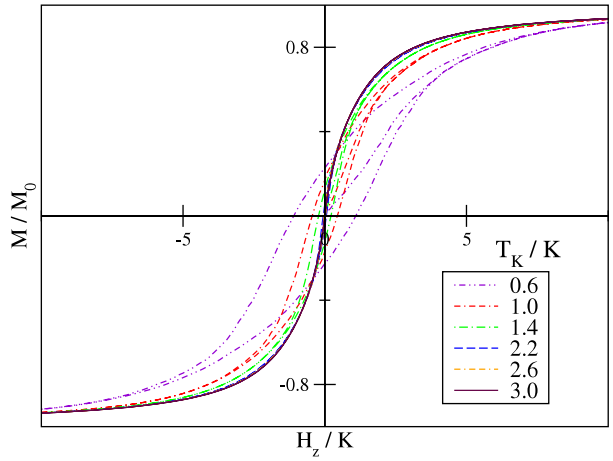

Figure 1. Hysteresis loops generated by sweeping the external field symmetrically.

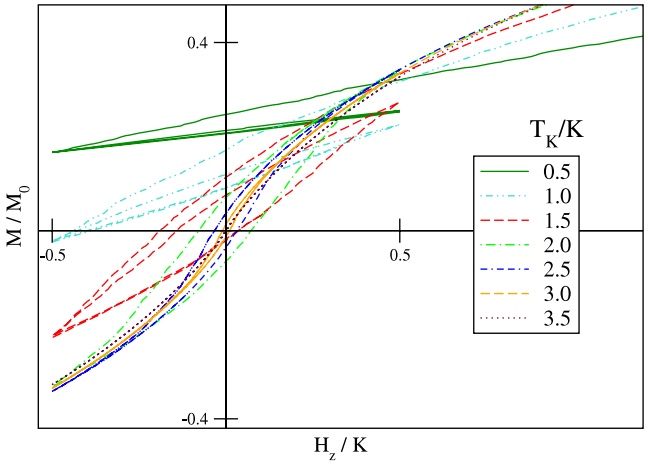

Figure 2. Displaced hysteresis loops generated by sweeping the external field asymmetrically.

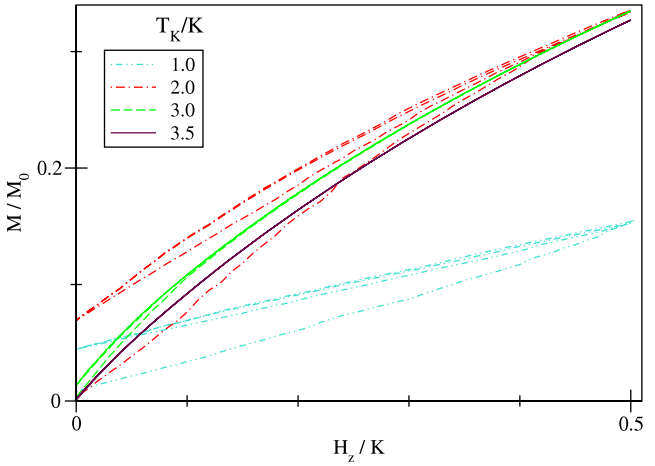

Figure 3. Minor hysteresis loops generated by sweeping the external field asymmetrically.

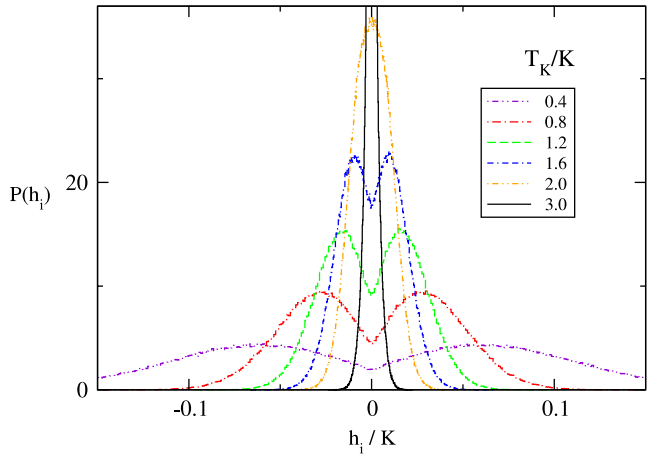

Figure 4. $\mathcal{P}(h_i)$ for various values of $T_{\rm K}$ in zero external field, $H_z = 0$.

$T_{\rm K} \simeq 3$. Hence, we see how the free-energy manifold goes from having many local minima (for small $T_{\rm K}$) to having a single minimum as the magnetic impurities become screened due to the Kondo effect.

More interesting, however, are the hysteresis loops in figure 2, which were obtained by sweeping the external fields asymmetrically. More specifically, these hysteresis curves were generated by preparing the impurity spins in a random configuration and in a large external magnetic field, $H_z/K = 6.0$; the external field was decreased to a negative value $H_z/K = -0.5$. Then the external field was increased to $H_z/K = +0.5$, and then decreased back to $H_z/K = -0.5$, thus generating a complete hysteresis loop. Here, we see the hysteresis loops are displaced along the y-axis for smaller values of $T_{\rm K}$. As $T_{\rm K}$ is increased, the hysteresis loops shift toward the origin and eventually become centered about the origin. Hence, for smaller values of $T_{\rm K}$, the system can maintain a permanent magnetization in addition to exhibiting hysteresis; for $T_{\rm K} > 2.0$, this permanent magnetization disappears. Eventually, the hysteretic behavior is lost for $T_{\rm K}$ large enough, $T_{\rm K} \simeq 3$ i.e. when the impurities become strongly screened by the conduction electrons.

Figure 3 shows further hysteresis loops for various values of $T_{\rm K}$. Here, as in figure 2, the field was swept asymmetrically. However, in this case the system was prepared in zero external field (as compared to figure 2, where the system was prepared in a large external field); then the external field was increased to a finite, positive value $H_z/K = 0.5$. The field was then decreased to zero and subsequently increased back to $H_z/K = 0.5$, thus generating a complete hysteresis loop. Here, we see so-called 'minor hysteresis loops'. These minor hysteresis loops persist until $T_{\rm K} \simeq 3.0$.

3.2. Distribution of fields

We now show results for the distribution of fields $\mathcal{P}(h_i)$. Figure 4 shows results for $\mathcal{P}(h_i)$ in zero external field for several values of $T_{\rm K}$. The results were generated by averaging over 100 realizations of the $\{K_{i,j}\}$. We see that for smaller values of $T_{\rm K}$, $\mathcal{P}(h_i)$ has maxima for $h_i \neq 0$. This occurs because the system lowers its energy when the impurity spins are aligned with the internal fields acting on them. (See equation (5).) As $T_{\rm K}$ increases—as the impurity spins are more

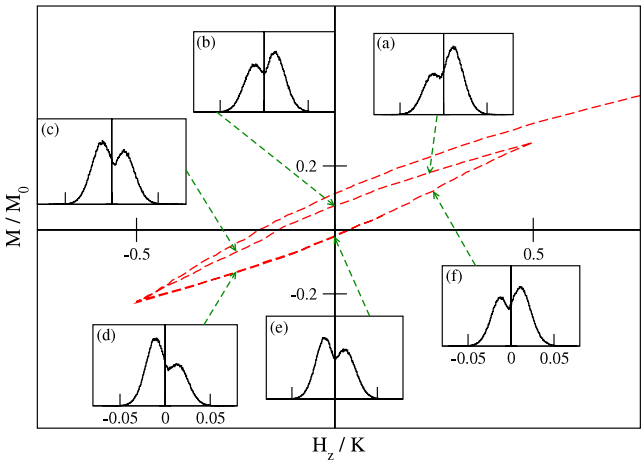

Figure 5. $\mathcal{P}(h_i)$ for $T_K = 1.5$ at various points along the hysteresis loop from figure 2.

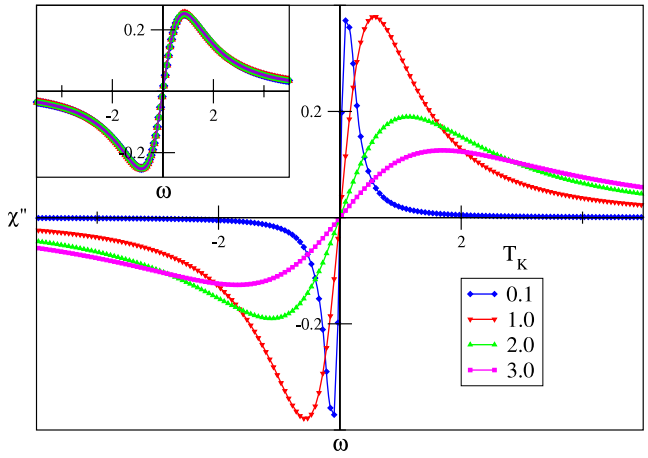

Figure 6. Main panel: χ'' for several values of T_K in zero external field ($H_z = 0$). Inset: χ'' at several points along the hysteresis curve.

strongly screened by the conduction electrons—the peaks in $\mathcal{P}(h_i)$ shift toward $h_i = 0$. This occurs because for $T_K \neq 0$, screening of the impurity spins due to the Kondo effect reduces the effective magnitude of their moments, and hence reduces the effective field they can produce. As a result, the probability for h_i at a site to be zero is increased. For T_K large enough, $\mathcal{P}(h_i)$ is peaked at $h_i = 0$ and has a Gaussian shape.

We now consider how the distribution of fields depends on the system's history. Figure 5 shows results for $\mathcal{P}(h_i)$ for $T_K = 1.5$ at various points along the hysteresis curve in figure 2. In general, we see that $\mathcal{P}(h_i)$ is not symmetric about $h_i = 0$ due to the finite magnetization—$M > 0$ ($M < 0$) gives rise to $\mathcal{P}(h_i)$ with more weight for $h_i > 0$ ($h_i < 0$). In particular, it is interesting to note that panels (b) and (e) have $H_z = 0$. However, $\mathcal{P}(h_i)$ in panel (b) ((e)) has more weight for $h_i > 0$ [$h_i < 0$], thus showing the importance of the system's history on $\mathcal{P}(h_i)$.

3.3. Impurity spin susceptibility

Having probed the free-energy manifold, we now turn to the impurity spins' dynamics; in particular, we consider the imaginary part of the impurity spin susceptibility $\mathrm{Im}[\chi(\omega, T)]$. This quantity could be measured in experiments which probe the impurity spins' excitation spectrum e.g. neutron scattering experiments. From equation (10), we obtain

$$\mathrm{Im}[\chi(\omega,T)] = \frac{1}{2\pi}\frac{T_K}{\omega^2+T_K^2}\left\{\mathrm{Im}\left[\psi(z_+)-\psi(z_-)\right] + \left(\frac{T_K}{\omega}\right)\mathrm{Re}\left[\psi(z_+)+\psi(z_-)-2\,\psi(z_0)\right]\right\}, \tag{12}$$

where $\psi(z)$ is the digamma function [14], and

$$z_0 = \left(\frac{1}{2}+\frac{T_K}{4\pi T}\right)+\frac{\mathrm{i}}{2\pi T}h_i,$$
$$z_\pm = \left(\frac{1}{2}+\frac{T_K}{4\pi T}\right)+\frac{\mathrm{i}}{2\pi T}(h_i \pm \omega).$$

In figure 6 we plot χ'', the imaginary part of the impurity spin susceptibility averaged over the distribution of fields,

$$\chi'' \equiv \int \mathrm{d}h_i\, \mathcal{P}(h_i)\,\mathrm{Im}[\chi(\omega, T=0)]. \tag{13}$$

The main panel in figure 6 shows χ'' versus ω for several values of T_K, with the external magnetic field set to zero, $H_z = 0$. The curves in figure 6 were obtained by taking the expression in equation (12) and averaging over the appropriate distribution of fields from figure 4. We see that χ'' has its maximum and minimum near $\omega = 0$ for the smallest value of T_K ($T_K = 0.1$). As T_K increases, the maximum and minimum in χ'' shifts away from $\omega = 0$ and becomes broader. It is interesting to note that $\mathcal{P}(h_i)$ is quite broad for small values of T_K, and its maxima are shifted away from $h_i = 0$. On the other hand, $\mathcal{P}(h_i)$ has most of its weight near $h_i = 0$ for larger values of T_K. However, the behavior of $\mathcal{P}(h_i)$ does not appear to be reflected in χ''. This occurs because we have taken the interimpurity interaction to be Ising-like—when $T_K \to 0$ the impurity spins have no dynamics. Hence, when $T_K \to 0$ all of the weight of χ'' is shifted toward $\omega = 0$.

The inset of figure 6 shows χ'' for $T_K = 1.5$ at several points along the hysteresis curve from figure 5. More specifically, the blue diamonds, red triangles, green squares, and violet circles were computed at points (a), (b), (d), and (e), respectively on the hysteresis curve from figure 5 (averaging equation (12) over the distribution of fields at those points). The curves are, for all practical purposes, indistinguishable.

4. Concluding remarks

To summarize, we discussed the influence of Kondo physics on the properties of a spin glass. By considering the hysteresis in the glass phase, we probed the complexity of the free-energy manifold and how it is affected by Kondo physics. In particular, we saw how the hysteretic behavior is lost as the impurities become screened and, concomitantly, the free-energy manifold becomes smoothed. Furthermore, we considered the impurity spin's dynamics in the glass phase

and how it is influenced by Kondo physics. Interesting future work would be to consider impurities with larger spins (rather than spin-1/2 impurities), as well as the RKKY and random Dzyaloshinskii–Moriya interactions.

Acknowledgments

This work was supported by the NSERC of Canada and a SHARCNET Research Chair.

References

[1] Hewson A 1993 *The Kondo Effect to Heavy Fermions* (Cambridge: Cambridge University Press)
[2] Kondo J 1964 *Prog. Theor. Phys.* **32** 37
[3] Ruderman M A and Kittel C 1954 *Phys. Rev.* **96** 99
Kasuya T 1956 *Prog. Theor. Phys.* **16** 45
Yosida K 1957 *Phys. Rev.* **106** 893
[4] Schopfer F, Bauerle C, Rabaud W and Saminadayar L 2003 *Phys. Rev. Lett.* **90** 56801
[5] Magalhaes S G, Zimmer F M, Krebs P R and Coqblin B 2006 *Phys. Rev.* B **74** 14427
Theumann A and Coqblin B 2004 *Phys. Rev.* B **69** 214418
Theumann A, Coqblin B, Magalhaes S G and Schmidt A A 2001 *Phys. Rev.* B **63** 54409
Parcollet O and Georges A 1999 *Phys. Rev.* B **59** 5341
Sengupta A M and Georges A 1995 *Phys. Rev.* B **52** 10295
[6] Fischer K H and Hertz J A 1991 *Spin Glasses* (Cambridge: Cambridge University Press)
[7] Soukoulis C M, Levin K and Grest G S 1983 *Phys. Rev.* B **28** 1495
[8] Soukoulis C M, Grest G S and Levin K 1983 *Phys. Rev.* B **28** 1510
[9] Thouless D J, Anderson P W and Palmer R G 1977 *Phil. Mag.* **35** 593
[10] Kao Y-J, Grest G S, Levin K, Brooke J, Rosenbaum T F and Aeppli G 2001 *Phys. Rev.* B **64** 60402(R)
[11] Barzykin V and Affleck I 2000 *Phys. Rev.* B **61** 6170
[12] Chamon C de C and Fradkin E 1997 *Phys. Rev.* B **56** 2012
[13] See, for example Gogolin A O *et al* 1999 *Bosonization Approach to Strongly Correlated Systems* (Cambridge: Cambridge University Press)
[14] Gradshteyn I S and Ryzhik I M 1994 *Table of Integrals, Series, and Products* (San Diego, CA: Academic)
Abramowitz M and Stegun I A 1965 *Handbook of Mathematical Functions* (New York: Dover)
[15] See Ling D D, Bowman D R and Levin K 1983 *Phys. Rev.* B **28** 262 and references therein
[16] Bray A J, Sompolinsky H and Yu C 1986 *J. Phys. C: Solid State Phys.* **19** 6389